J|A|C|S
ARTICLES
Published on Web 01/30/2003

Design of Triple Helix Forming C-Glycoside Molecules

Jian-Sen Li,[†] Yun-Hua Fan,[†] Yi Zhang,[†] Luis A. Marky,[†,‡] and Barry Gold*[,†,‡]

Eppley Institute for Research in Cancer and Department of Pharmaceutical Sciences, University of Nebraska Medical Center, 986805 Nebraska Medical Center, Omaha, Nebraska 68198-6805

Received August 6, 2002; E-mail: bgold@unmc.edu

Abstract: The modeling, synthesis, and characterization of oligomers containing 2-aminoquinazolin-5-yl 2′-deoxynucleotide residues are reported. The 2-aminoquinazoline residues sequence specifically bind via Hoogsteen base pairing as a third strand in the center of the major groove at T:A base pair Watson−Crick duplex sequences. Evidence for the formation of a sequence specific three-stranded structure is based on thermal denaturation UV−vis and fluorescence studies. The novel 2-aminoquinazoline C-nucleotide is a component of a system designed to overcome the homopurine requirement for triple helix structures.

Targeting DNA sequences via formation of triple helical structures is an attractive approach to specifically regulate gene expression.[1] Unfortunately, the utility of triple helix mediated antigene strategies has been limited by the requirement that the triplex-forming oligomer (TFO) recognize and bind exclusively to purine bases in duplex Watson−Crick DNA. This restricts the formation of triple-stranded structures in both the pyrimidine[1a,2] and purine[3] motifs to homopurine regions of DNA (Figure 1). One of the critical reasons for this homopurine strand requirement is that the third strand binds asymmetrically in the major groove. The asymmetric binding arrangement makes it impossible for the third strand to traverse from a purine on one side of the major groove to a purine on the complementary strand in a hetero sequence (Figure 2). In addition, even if the backbone of the third strand could accommodate the movement across the groove, there would be a concomitant change in strand polarity and pyrimidine motif TFO's bind in a parallel orientation relative to the purine-rich strand (Figure 1). Despite some ingenious attempts, general and practical strategies to circumvent the triple helix requirement have been of limited success.[4]

Herein, we report an approach to target hetero purine-pyrimidine sequences using oligomers (OLs) composed of unnatural C-glycoside bases that recognize purines by Hoogsteen base pairing schemes but whose glycosidic bond is (i) located near the center of the major groove and (ii) perpendicular to the Watson−Crick H-bonds of the duplex target (Figure 3). The central location and directionality of the linkage between the modified base and the backbone eliminates the traversing problem (Figure 4). In addition, the use of different modified bases to specifically recognize T:A vs A:T and C:G vs G:C Watson−Crick pairing (Figure 3) eliminates the strand polarity issue since the third strand reads in one direction purine information in the major groove on either strand.

To test the feasibility of the design, the synthesis of the antiTA phosphoramidite and its incorporation into oligomers (Table 1 for sequences) are presented along with UV−vis and fluorescence melting profiles. Our results suggest that the incorporation of the antiTA C-glycoside into oligonucleotides results in the formation of sequence-specific intramolecular triple helix structures.

Experimental Section

General. All ^{1}H NMR were recorded on a Varian 500 MHz instrument. Mass spectral analyses were performed at the Washington University Mass Spectroscopy Source (St. Louis, MO) and the Midwest Center for Mass Spectroscopy at the University of Nebraska−Lincoln (Lincoln, NE). All reagents were of the highest purity and used as is unless specified otherwise.

Molecular Modeling. Duplex $d(T)_4$:$d(A)_4$ DNA was built using Arnott coordinates[5] in the Biopolymer module of SYBYL (Tripos Associates, St. Louis, MO). An anti$(TA)_4$ strand was constructed in the Build module by changing the thymines of $d(T)_4$ to quinazolines. The structures of the heterocycles in the constructed anti$(TA)_4$ oligomer were minimized using the Kollman Force Field[6] (as implemented in SYBYL) with the deoxyribose phosphate backbone treated as an aggregate. The antiTA strand and the duplex, treated as separate aggregates, were gradually docked with each other using Hoogsteen H-bonding distance and angle constraints and a distance-dependent dielectric $\epsilon = R_{i,j}$.

[†] Eppley Institute for Research in Cancer.
[‡] Department of Pharmaceutical Sciences.

(1) (a) Moser, H. E.; Dervan, P. B. *Science* **1987**, *238*, 645−650. (b) Maher, L. J., III; Wold, B.; Dervan, P. B. *Science* **1989**, *245*, 725−230. (c) Thuong, N. T.; Hélène, C. *Angew. Chem., Int. Ed. Engl.* **1993**, *32*, 6−690. (d) Praseuth, D.; Guieysse, A. L.; Hélène, C. *Biochim. Biophys. Acta* **1999**, *1489*, 181−206. (e) Fox, K. *Curr. Med. Chem.* **2000**, *7*, 17−37.
(2) (a) Felsenfeld, G.; Davies, D. R.; Rich, A. *J. Am. Chem. Soc.* **1957**, *79*, 2023−2024. (b) Morgan, A. R.; Wells, R. D. *J. Mol. Biol.* **1968**, *37*, 63−80. (c) Lee, J. S.; Johnson, D. A.; Morgan, A. R. *Nucl. Acids Res.* **1979**, *6*, 3073−3091.
(3) (a) Broitman, S. L.; Im, D. D.; Fresco, J. Y. *Proc. Natl. Acad. Sci. U.S.A.* **1987**, *84*, 5120−5124. (b) Cooney, M.; Czernuszewicz, G.; Postel, E. H.; Flint, S. J.; Hogan, M. E. *Science* **1988**, *241*, 456−459. (c) Kohwi, Y.; Kohwi-Shigematsu, T. *Proc. Natl. Acad. Sci. U.S.A.* **1988**, *85*, 3781−3785. (d) Beal, P. A.; Dervan, P. B. *Science* **1991**, *251*, 1360−1363.
(4) (a) Horne, D. A.; Dervan, P. B. *J. Am. Chem. Soc.* **1990**, *112*, 2435−2437. (b) Jayasena, S. D.; Johnston, B. H. *Nucl. Acids Res.* **1992**, *20*, 5279−5288. (c) Gowers, D. M.; Fox, K. R. *Nucl. Acids Res.* **1999**, *27*, 1569−1577.
(5) Arnott, S.; Hukins, D. W. L. *Biochem. Biophys. Res. Commun.* **1972**, *47*, 1504−1509.
(6) Weiner, S. J.; Kollman, P. A.; Case, D. A.; Singh, U. C.; Ghio, C.; Alagona, G.; Profeta, S., Jr.; Weiner, P. *J. Am. Chem. Soc.* **1984**, *106*, 765−784.

10.1021/ja028033x CCC: $25.00

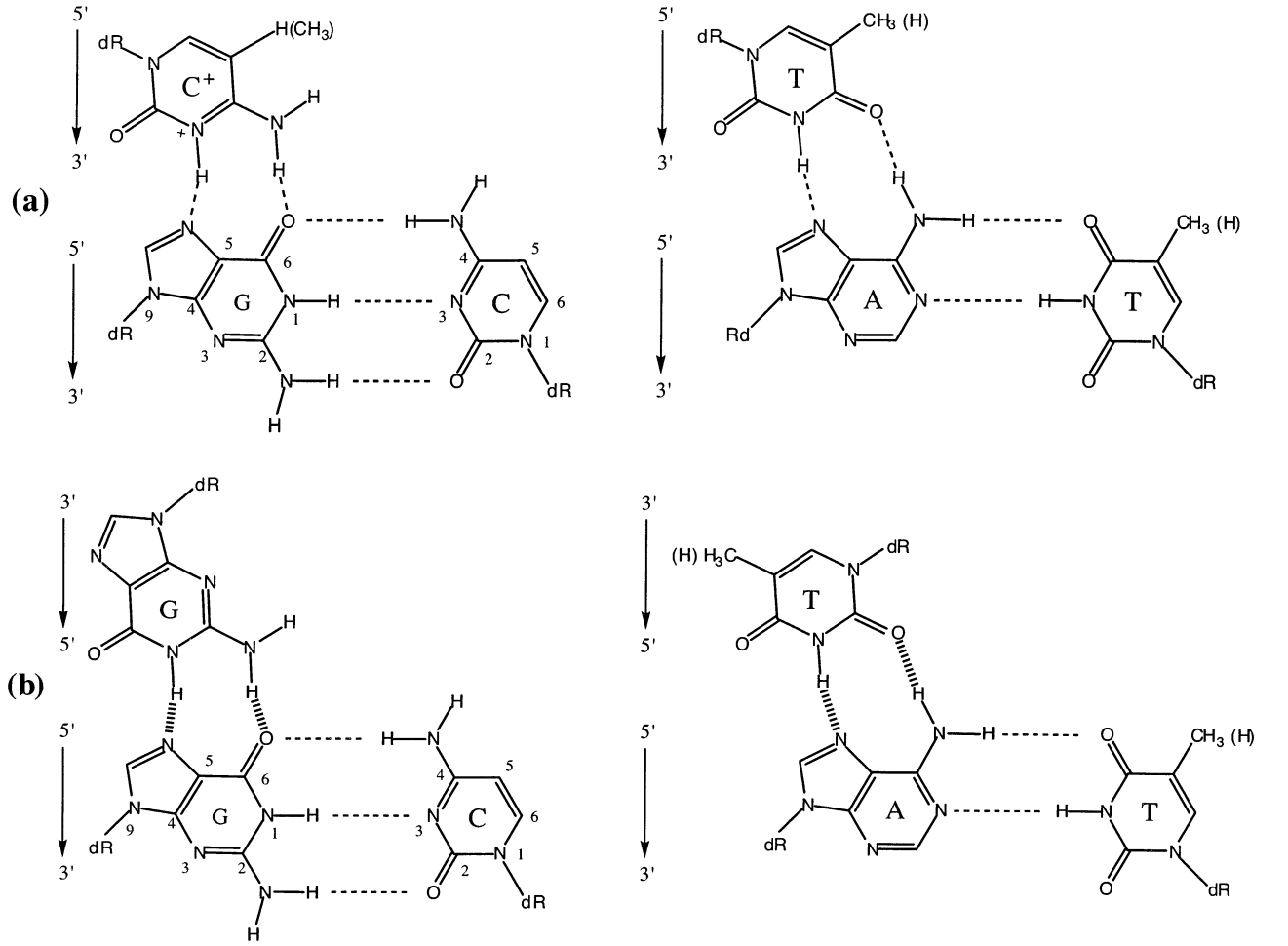

Figure 1. (a) Pyrimidine motif with third strand parallel to purine strand and (b) purine motif with third strand antiparallel to the purine strand.

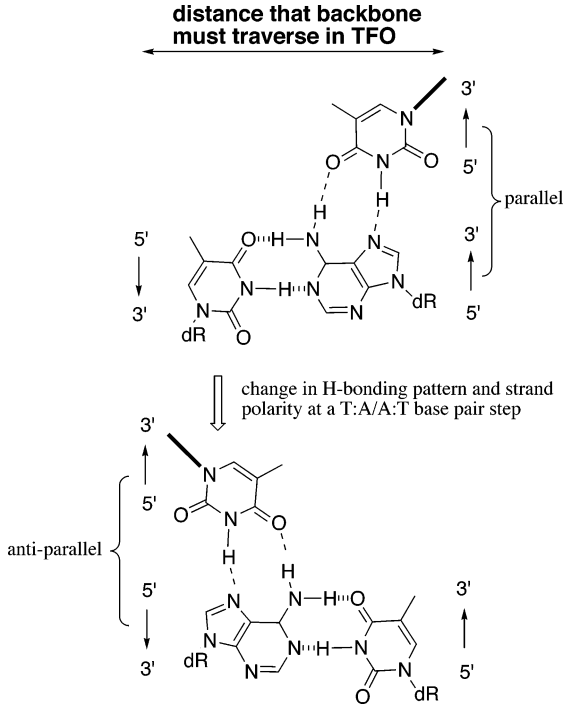

Figure 2. Required change in strand polarity and movement of a pyrimidine motif TFO backbone between complementary strands in duplex DNA at a 5′-T:A/A:T base pair step (darkened bonds represent the attachment to the sugar−phosphate backbone).

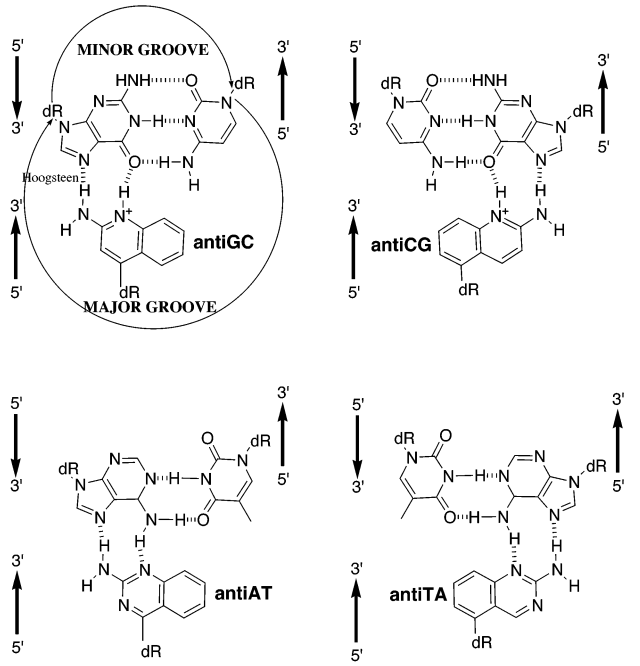

Figure 3. Hoogsteen H-bonding of antiTA, antiAT, antiCG, and antiGC C-glycosides to their duplex Watson−Crick partners.

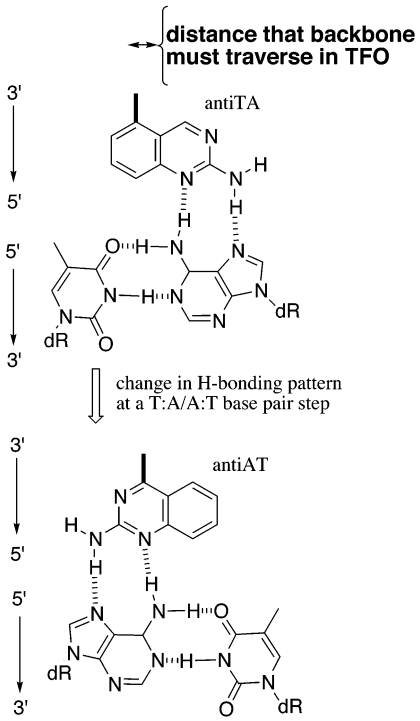

Figure 4. Association of an antiTA and antiAT in a TFO with duplex DNA at a 5′-T:A/A:T base pair step (darkened bonds represent the attachment to the sugar−phosphate backbone).

Table 1. Sequences of Oligomers and Their T_M Values (°C) at 260 and 350 nm

OL-1: 5′-d([antiTA]$_6$-C_5-T_6-C_5-A_6)
OL-2: 5′-d([antiTA]$_6$-C_5-A_6-C_5-T_6)
OL-3: 5′-d(T_6-C_5-T_6-C_5-A_6)
OL-4: 5′-d(T_6-C_5-A_6-C_5-T_6)
OL-5: 5′-d([antiTA]$_6$-C_5-T_2AT_3-C_5-A_3-T-A_2)
OL-6: 5′-d(C_5-T_6-C_5-A_6)
OL-7: 5′-d(C_5-A_6-C_5-T_6)

		260 nm		350 nm	
		netropsin equivalents[b]		netropsin equivalents[b]	
oligomer	NaCl (mM)	0	1	0	1
OL-1	50	26.3	57.3	24.7	25.3
	200	35.2	56.6	26.4	26.7
OL-2	50	23.9	53.6	n.d.[c]	n.d.
	200	29.8	55.7	n.d.	n.d.
OL-3	50	22.7	(8.5) 54.4	n.d.	n.d.
	200	32.1	(13.0) 59.4	n.d.	n.d.
OL-4	50	24.5	58.1	n.d.	n.d.
	200	32.1	62.2	n.d.	n.d.
OL-5	50	20.5	50.1	n.d.	n.d.
	200	29.5	45.8	n.d.	n.d.
OL-6	50	25.3	55.4	n.d.	n.d.
	200	29.8	60.0	n.d.	n.d.
OL-7	50	24.8	57.9	n.d.	n.d.
	200	25.2	59.4	n.d.	n.d.

[a] Values (±1 °C) based on shape analysis [ref 8]: 10 mM NaH_2PO_4 buffer (pH 7.0) containing either 50 or 200 mM NaCl. The values in parentheses are triplex to duplex transition. [b] Netropsin equivalents relative to equivalents of oligomer strand. [c] n.d. = not detected.

2-Bromo-6-nitrobenzaldehyde (2). Br_2 (10 mL) was added to 2-bromo-6-nitrotoluene (25 g) in a three-necked 500 mL flask and the mixture heated at 145−150 °C (oil bath temperature) over 2 h while the reaction was illuminated with an 800 W sun lamp. After the addition of Br_2, the reaction was illuminated for an additional 2 h. The reaction was allowed to cool, and EtOH (35 mL) was added followed by the addition of pyridine (25 mL). The final mixture was heated in a boiling water bath to induce precipitation of the product. After 1 h, the precipitate was filtered and washed with cold EtOH (100−250 mL) and air-dried. The final product was an off-white crystal (33 g).

The benzyl bromide derivative (33 g, 88.7 mmol) obtained from the previous step was mixed with *N*,*N*-dimethyl-*p*-nitrosoaniline (23 g, 153.0 mmol) and EtOH (400 mL) in an ice bath. After the reaction had cooled for 10 min, 1 N NaOH (250 mL) was added. The mixture was stirred at 0 °C for 2 h and the product filtered and washed with water (200 mL) and dried. The yellow nitrone powder (40 g) was used for the next reaction without further purification.

The nitrone (40 g) synthesized from the last step was mixed with 6 N H_2SO_4 (300 mL) and the mixture heated for 10 min in a boiling water bath. The 2-bromo-6-nitrobenzaldehyde product was filtered and washed with cold water (400 mL) until the rinse was light in color. The desired product was an off-white powder (20.6 g), mp 78−80 °C, which was used without further purification: ^{1}H NMR ($CDCl_3$) δ 7.53 (dd, J = 8.0, 7.5,1 H), 7.92 (d, J = 8.0, 1 H), 8.02 (d, J = 7.5, 1 H), 10.28 (s, 1 H).

2-Bromo-6-aminobenzaldehyde (3). A mixture of concentrated HCl (32 mL) and water (65 mL) was added to *2* (5 g, 21.9 mmol). The mixture was heated for 10 min in a boiling water bath; then iron (2.56 g, 45.7 mmol) was added to the hot mixture. The mixture was stirred for another 10 min in the hot water bath after which time ice was added. Then CH_2Cl_2 (30 mL) was added to dissolve the insoluble viscous liquid that formed in the aqueous solution. The mixture was filtered quickly and the organic layer collected. The remaining aqueous layer was then neutralized with concentrated NH_4OH and extracted with CH_2Cl_2. The combined CH_2Cl_2 extract was concentrated under reduced pressure to afford **3** which was used without further purification.

2-Amino-5-bromoquinazoline (4). Na metal (0.52 g) was dissolved in 2-ethoxyethanol (40 mL) and then guanidine·HCl (2.07 g) was added. The reaction turned cloudy and was stirred for another 10 min at room temperature. The reaction was filtered and the solid washed with a small amount of 2-ethoxyethanol. The filtrate was mixed with **3** and the mixture heated (160−180 °C) with stirring until most of the solvent had evaporated. Then MeOH (20 mL) was added to the resulting solid, and the solution refluxed for 2 h. Silica gel (20 g) was then added into this solution and the solvent removed under reduced pressure. The resulting solid was further dried by heating in an oven (120 °C) for 1 h. The crude product absorbed onto silica gel was placed into a dropping funnel pre-loaded with fresh silica gel (25 g). This silica gel "column" was first extracted with CH_2Cl_2/hexanes (1:1, 100 mL) for 4−6 h and then extracted with CH_2Cl_2 (100 mL) for 8−12 h. All the extracts were monitored by TLC. The column was finally extracted with CH_2Cl_2/Et_2O (1:1, 100 mL) for 12−24 h until TLC analysis indicated that no more product was left on the column. Removal of the solvent furnished the product (0.88 g, 18% yield) in 85−95% purity. This material can be used for the next reaction without any further purification. It could be recrystallized from CH_2Cl_2/Et_2O to furnish an off-white powder (0.45 g) in >99% purity: mp, 248−249 °C (dec); ^{1}H NMR (DMSO-d_6) δ 7.11 (bs, 2 H, NH_2), 7.41 (d, J = 7.5,1 H), 7.47 (d, J = 6.5, 1 H), 7.55 (dd, J = 7.5, 6.5, 1 H), 9.15 (s, 1 H); MS (FAB) *m*/*z* 224 (M) and 225 (M + 1).

(2′*R*)-*cis*-5-[2′,5′-Dihydro-4′-((*tert*-butyldiphenyl)silyl)oxy-2′-furanyl]-2-aminoquinazoline (5). 4 (0.74 g) and 1,4-anhydro-2-deoxy-3-*O*-(*tert*-butyldiphenylsilyl)-D-*erythro*-pent-1-enitol[7] (1.35 g) were dissolved in THF (80 mL) under N_2. Then a catalytic amount of bis-(dibenzylideneacetone)Pd(0) (0.45 g) and tri(*tert*-butyl)phosphine (0.5 mL) were added to the reaction. After the reaction had been purged with N_2 for 5 min, Et_3N (7.5 mL) was added. The final mixture was then refluxed overnight under N_2. The reaction was cooled and filtered and the filtrate concentrated under reduced pressure. The residue was subjected to flash chromatography (EtOAc) to furnish a dark-red viscous liquid as the final product (0.84 g, 51% yield): ^{1}H NMR ($CDCl_3$) δ 1.10 (s, 9 H), 3.78 (bs, 2 H, C5′H, C5′′H), 4.46 (s, 1 H, C4′H), 4.84 (s,

(7) Farr, R. N.; Davies, G. D., Jr. *Carbohydr. Chem.* **1990**, *9*, 653−660.

1 H, C5′OH), 5.16 (bs, 2 H, NH_2), 6.24 (d, J = 6.5, 1 H, C1′H), 6.52 (d, J = 6.5, 1 H, C2′H), 7.38−7.53 (m, 10 H), 7.80−7.86 (m, 3 H), 9.38 (s, 1 H).

5-[β-D-Glyceropentofuran-3′-ulos-1′-yl]-2-aminoquinazoline (6). Tetrabutylammonium fluoride (3.5 mL, 1 M in THF) was added to a cooled (ice bath) solution of nucleoside **5** in THF (10 mL). Then a catalytic amount of concentrated AcOH (250 μL) was added and the reaction stirred at 0 °C under N_2 for 1 h and then concentrated under reduced pressure. The product was purified by flash chromatography (EtOAc: MeOH, 9:1). The final product was a pale ivory colored powder (0.43 g, 98% yield): ^{1}H NMR (DMSO-d_6) δ 2.98 (dd, J = 12.0, 5.5, 2 H, C2′H, C2″H), 3.69−3.72 (m, 2 H, C5′H, C5″H), 4.08 (t, J = 3.1, 1 H, C4′H), 5.81 (dd, J = 5.0, 5.5, 1 H, C1′H), 6.80 (s, 2 H, NH_2), 7.38 (d, J = 7.5, 1 H), 7.45 (d, J = 6.5, 1 H), 7.65 (dd, J = 7.5, 6.5, 1 H), 9.46 (s, 1 H); HRMS (FAB) m/z 259.0960 (M^+), 259.0957 (calcd).

5-[2′-Deoxy-β-D-*threo*-pentofuranosyl]-2-aminoquinazoline (7). Ketone **6** (0.65 g) was dissolved in 80 mL of AcOH:CH_3CN (1:1) and stirred under N_2 at −23 °C (dry ice/CCl_4). $NaHB(OAc)_3$ (0.6 g) was added to the cooled solution and the mixture stirred under N_2 at −23 °C for 1 h at which time 3% H_2O_2 (0.5 mL) was added. The reaction was concentrated and stirred with Na_2CO_3 (3 g) in 10 mL of CH_2Cl_2/MeOH (1:1) at room temperature for 1 h. The product was purified by flash chromatography with EtOAc:MeOH (4:1). The final product was obtained as a pale yellow powder (0.38 g, 59% yield): ^{1}H NMR (DMSO-d_6) δ 1.90−1.95 (m, 1 H, C2′H), 2.25−2.28 (m, 1 H, C2″H), 3.46−3.55 (m, 2 H, C5′H, C5″H), 3.86 (dd, J = 3.0, 5.0, 1 H, C4′H), 4.23 (br s, 1 H, C3′H), 5.66 (dd, J = 4.5, 6.0, 1 H, C1′H), 6.78 (s, 2 H, NH_2), 7.31 (d, J = 7.5, 1 H), 7.33 (d, J = 8.5, 1 H), 7.61 (dd, J = 8.5, 7.5, 1 H), 9.34 (s, 1 H); HRMS (FAB) m/z 262.1189 (MH^+), 262.1192 (calcd).

N^2-Isobutyryl-5-[2′-deoxy-β-D-*threo*-pentofuranosyl]-2-aminoquinazoline (8). Alcohol **7** (0.38 g) was dissolved in dry pyridine (20 mL) and cooled in an ice bath. Then TMS-Cl (1 mL) was added to the cooled solution under N_2. The reaction was stirred at 0 °C for 30 min at which time isobutyric anhydride (1.3 mL) was added and the reaction stirred for an additional 2 h at room temperature. After 2 h, the reaction was again cooled in an ice bath and 2.5 mL of cold water added. The reaction was stirred for another 15 min; then concentrated NH_4OH (2.5 mL) was added to give a final concentration of approximately 2 M in ammonia. This mixture was stirred for another 30 min in an ice bath and then concentrated under reduced pressure to afford an oil. The oil was dissolved in a very small amount of water, which was washed with Et_2O. The aqueous layer was collected and concentrated and the residue purified by flash chromatography (EtOAc:MeOH, 9:1) to give the desired product as a yellow powder (0.3 g, 63% yield): ^{1}H NMR (DMSO-d_6) δ 1.12 (d, J = 7.0, 6 H), 1.95−2.01 (m, 1 H, C2′H), 2.31−2.35 (m, 1 H, C2″H), 2.88−2.94 (m, 1 H), 3.50−3.60 (m, 2 H, C5′H, C5″H), 3.91 (dd, J = 3.0, 5.0, 1 H, C4′H), 4.26 (bs, 1 H, C3′H), 4.86 (t, J = 5.5, 1 H, C5′OH), 5.19 (d, J = 4.0, 1 H, C3′OH), 5.77 (dd, J = 4.5, 6.0, 1 H, C1′H), 7.67 (d, J = 7.5, 1 H), 7.70 (d, J = 8.5, 1 H), 7.89 (dd, J = 8.5, 7.5, 1 H), 9.71 (s, 1 H), 10.68 (s, 1 H); HRMS (FAB) m/z 331.1532 (M^+), 331.1535 (calcd).

N^2-Isobutyryl-5-[2′-deoxy-β-D-*threo*-pentofuranosyl-5′-*O*-(4,4′-dimethoxytrityl)]-2-aminoquinazoline (9). Dry **8** (0.215 g) was dissolved in anhydrous pyridine (5 mL) under N_2. Then 4,4′-dimethoxytrityl chloride (0.28 g), DMAP (6 mg), and Et_3N (0.2 mL) were added to the solution at room temperature. After 5 h, additional aliquots of 4,4′-dimethoxytrityl chloride, DMAP, and Et_3N were added. The reaction was stirred under N_2 at room temperature for a total of 24 h and the reaction concentrated under reduced pressure and quickly flash chromatographed (EtOAc containing 1% Et_3N). The final product was a white powder (0.25 g, 61% yield): ^{1}H NMR (DMSO-d_6) δ 1.12 (d, J = 7.0, 6 H), 2.07−2.10 (m, 1 H, C2′H), 2.41−2.44 (m, 1 H, C2″H), 2.91−2.95 (m, 1 H), 3.12−3.19 (m, 2 H, C5′H, C5″H), 3.72 (s, 6 H), 4.01−4.05 (m, C4′H), 4.22 (bs,1 H, C3′H), 5.25 (d, J = 4.5, 1 H, C3′OH), 5.89 (dd, J = 4.0, 7.5, 1 H, C1′H), 6.86 (d, J = 9.0, 4 H), 7.20−7.28 (m, 7 H), 7.38 (d, J = 8.5, 2 H), 7.65 (d, J = 7.5, 1 H), 7.72 (d, J = 8.5, 1 H), 7.87 (dd, J = 7.5, 8.5, 1 H), 9.69 (s, 1 H), 10.70 (s, 1 H); HRMS (FAB) m/z 656.2735 ([M + Na]$^+$), 656.2737 (calcd).

N^2-Isobutyryl-5-[2′-deoxy-β-D-*threo*-pentofuranosyl-3′-*O*-(2-cyanoethoxy)(diisopropylamino)phosphino-5′-*O*-(4,4′-dimethoxytrityl)]-2-aminoquinazoline (10). Dry trityl compound **9** (95 mg) was dissolved in dry CH_2Cl_2 (4 mL) and cooled in an ice bath under N_2. Then Hunig base (120 μL) was added followed by 2-cyanoethyl-*N*,*N*-diisopropylphosphoramidite (60 μL). The reaction was stirred at 0 °C for 10 min and then at room temperature for 1 h. The final reaction was concentrated under reduced pressure and the residue chromatographed (Et_2O containing 1% Et_3N). The final product was a white powder (0.1 g, 79% yield): ^{1}H NMR (DMSO-d_6) δ 1.12 (d, J = 7.0, 6 H), 1.17−1.28 (m, 12 H), 2.07−2.10 (m, 1 H, C2′H), 2.46−2.48 (m, 1 H), 2.50−2.54 (m, 1 H, C2″H), 2.65−2.68 (m, 1 H), 3.30−3.36 (m, 2 H, C5′H, C5″H), 3.50 (dd, J = 7.5, 6.5, 1 H), 3.50−3.68 (m, 4 H), 3.78 (s, 6 H), 4.32 (bs, 1 H, C4′H), 4.59 (bs,1 H, C3′H), 5.84 (m, 1 H, C1′H), 6.78 (m, 4 H), 7.20−7.35 (m, 7 H), 7.43−7.46 (m, 2 H), 7.69 (m, 1 H), 7.70−7.80 (m, 2 H), 8.04 (s, 1 H), 9.65 (s, 1 H); HRMS (FAB) m/z 856.3837 ([M + Na]$^+$), 856.3815 (calcd).

Oligonucleotide Synthesis and Purification. The synthesis of the oligomers was performed on a 200 nmol scale using standard solid-phase phosphoramidite methodology on an ABI 394 instrument. For 200 nmol scale synthesis, a 0.1 M MeCN solution of phosphoramidite (**10**) was used. On the basis of preliminary runs, the coupling time was set to 7 min with greater than 99% coupling efficiency as determined by trityl assay. After the synthesis, the resin inside the cartridge was mixed with 1 mL of concentrated NH_4OH, placed in a sealed bottle, and deprotected at 55 °C for 8 h. The crude oligomers were purified by HPLC: flow rate, 4 mL/min; solvent, 0.1 M TEAA (pH 7.0)/MeCN (9:1) for 10 min, to 0.1 M TEAA (pH 7.0)/MeCN (3:2) over 15 min, and then to 100% MeCN over 5 min. The HPLC fractions containing the oligomer were combined and lyophilized and the residue detritylated with 80% acetic acid solution (30 μL per OD) at room temperature for 20 min. The final product was purified on a Sephadex G-25M column. The products were analyzed by MALDI-MS.

Thermal Denaturation Studies. Melting curve transition measurements were performed on an AVIV 14 DS UV/vis spectrophotometer equipped with an IBM computer as thermoprogrammer. Oligomers (3−6 μM) were dissolved in 10 mM sodium phosphate (pH 7.0) containing 50 or 200 mM NaCl, and when specified with netropsin. The oligomers were heated to 80 °C and slowly cooled to 0 °C and held at that temperature for 30 min. The temperature was scanned from 0 to 80 °C at a heating rate of 0.2 °C/min with data-point collection in intervals of 0.2 °C. Below 20 °C, the cell compartment was flushed with N_2 to avoid condensation of water on the UV cells. The unfolding of the oligomers were measured by the change in absorbance at 260 and 350 nm versus temperature. The transition temperature T_M was determined by shape analysis of the melting curves.[8]

Fluorescent Studies. Fluorescence emission spectra were recorded from 330 to 600 nm with data-point collection in intervals of 2 nm on an AVIV Automated Titrating Differential/Ratio Spectroflurometer (Model ATF105) with a fixed excitation wavelength at 350 nm. The emission and excitation slits were set at 5 nm. DNA melting curve transitions measured by fluorescence change as a function of temperature were conducted with the same spectroflurometer with a fixed excitation wavelength at 350 nm and a fixed emission wavelength at 425 nm. OL-1, -2, and -5 (3−6 μM) and ketone **6** (4 μM) were dissolved in 10 mM sodium phosphate buffer (pH 7.0) containing 200 mM NaCl. The oligomers were heated to 75 °C, then slowly cooled to 0 °C, and held at 0 °C for 1 h. The temperature was scanned from 0 to

(8) Marky, L. A.; Breslauer, K. J. *Biopolymers* **1987**, *26*, 1601−1620.

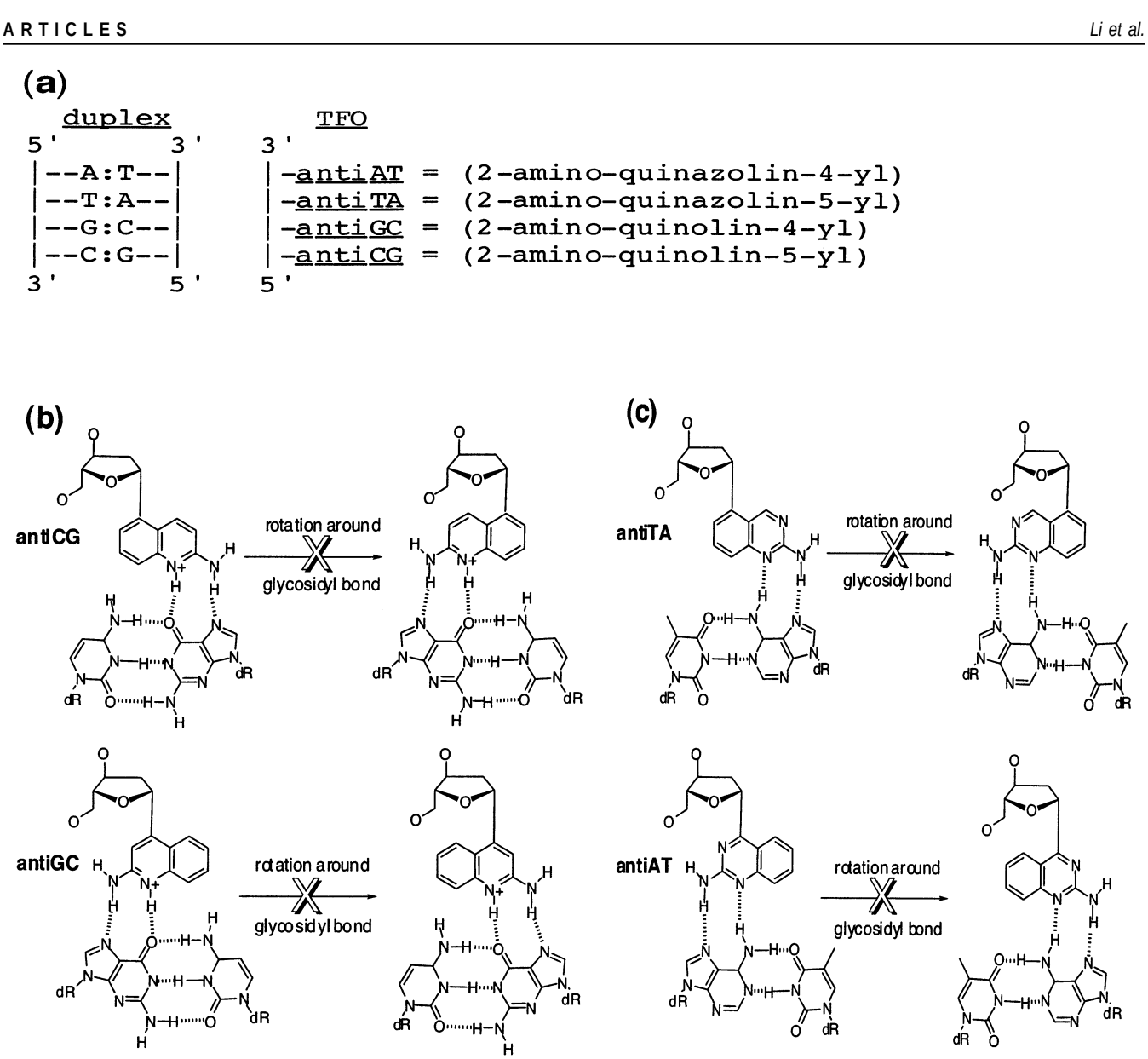

Figure 5. Terminology used to define how antiTA, antiAT, antiCG, and antiGC are designed to read Hoogsteen H-bonding information in Watson−Crick duplex DNA: (a) T:A base pair is arbitrarily defined by the T being in the left strand that runs 5′-3′ from top to bottom (A:T would have the A in the left strand); (b) conversion of the *anti*-conformation of the quinoline ring to the *trans* form is highly disfavored so the quinoline ring in antiCG or antiGC cannot rotate to become pseudo-equivalent to antiGC or antiCG, respectively; and (c) the same argument applies to antiAT and antiTA.

75 °C at a rate of 1 °C/min with data-point collection in intervals of 1 °C. Below 20 °C, the cell compartment was flushed with N_2 to avoid condensation of water on the fluorescence cell. The fluorescence change was normalized before it was plotted as a function of temperature.

Circular Dichroism Studies. Circular dichroism (CD) studies were performed using an AVIV 202 SF CD spectrometer. Oligomers (6−10 μM) were studied at 0 °C in 50 mM sodium phosphate buffer (pH 7.0). Samples were heated to 80 °C for 5 min and cooled to 4 °C over 60 min before spectra were collected. Rectangular optical cells with path lengths of 1 cm were used for DNA samples. The data are expressed as deg M^{-1} cm^{-1}.

Results and Discussion

Terminology. The heterocyclic C-glycoside "bases" in Figure 3 are designated as antiAT, antiTA, antiGC, and antiCG on the basis of their Watson−Crick duplex targets. Because these molecules are designed to recognize heteropurine/pyrimidine sequences in duplex DNA (even though only the purine base is read), their orientation has been *arbitrarily* defined relative to duplex DNA using the following convention: right-handed duplex DNA is viewed looking into the major groove with the strand on the viewer's left running 5′ to 3′ going from top to bottom. The TFO runs antiparallel (3′ → 5′) against the left strand of the duplex which runs 5′ → 3′ (Figure 5a). The antiTA will bind in the major groove if the base in the left strand is T, while antiAT will bind if the base is an A.

Strategy. The formation of a stable classical triple helix with hetero-purine/pyrimidine sequences is not possible because the information recognized in ds-DNA by the TFO moves from a point near the glycosidyl-N atom of the backbone of one strand of the duplex to a location approximately the same distance from the backbone on the complementary strand. Thus, to read a purine on the complementary strand, the backbone of the TFO must traverse a distance of ∼10 Å across the major groove (Figure 2). *This is not possible with a normal 5′-3′ sugar−phosphate backbone.* The tactic of having the glycosidic bond perpendicular to the H-bonding atoms of the C-glycoside

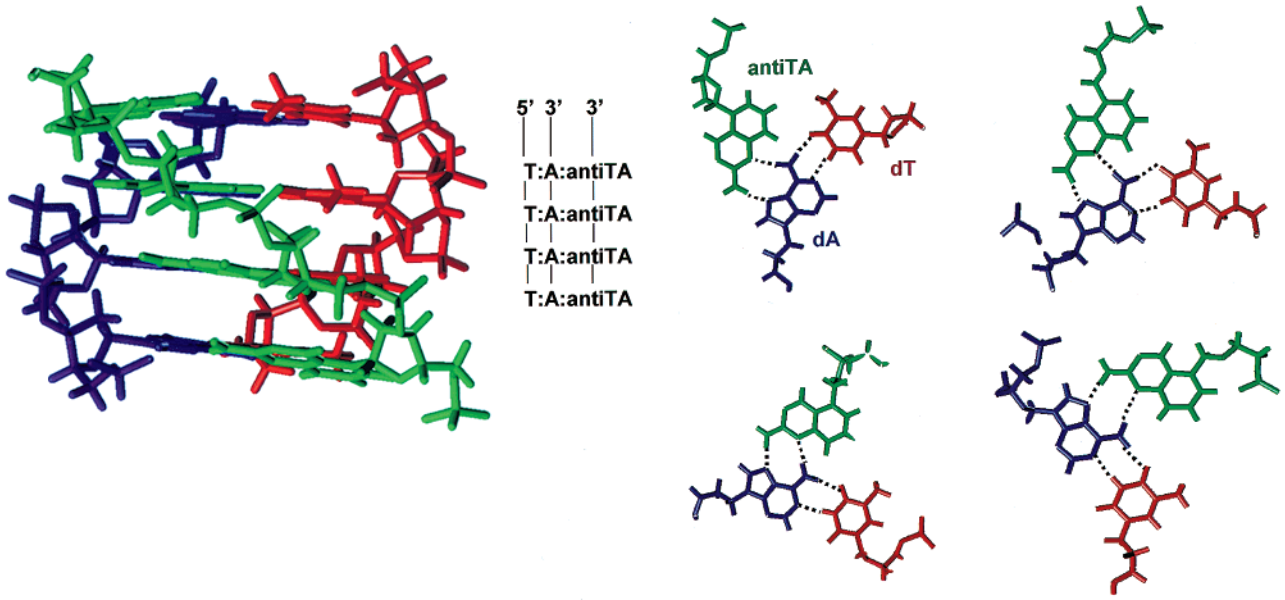

Figure 6. Modeling of (antiTA)$_4$ with d(T)$_4$:d(A)$_4$ duplex (color code: green, antiTA; blue, dA; red, dT): (left) side view looking into major groove; (right) orthogonal view down the long axis of DNA. Dotted bonds indicate atoms that are of the proper distance and alignment to form H-bonds.

heterocycles and the attachment at the C-4 (antiGC and antiAT) or C-5 (antiCG and antiTA) position results in locating the glycosidic bond in the TFO approximately 5.5 Å from the glycosidyl-N of the purine. Therefore, in a heteropurine/pyrimidine sequence the TFO has to traverse ~1−2 Å across the major groove as illustrated in Figure 4 at a T:A/A:T step. The central location of the glycosidic bond also avoids the problem of changing strand polarity since the C-glycoside TFO reads purine information on either strand in a single direction of the duplex.

The quinoline compounds antiGC and antiCG (Figure 3) were conceived to specifically recognize a G:C and a C:G base pair, respectively, as defined in Figure 5a. The quinolines have pK_a's of ~7.3[9] ensuring that the ring nitrogen is ionized at physiological pH, which allows it to form two H-bonds with the proper orientation. The specificities of the Hoogsteen recognition patterns of the quinolines in a TFO are due to their preference for the *anti*-conformation with respect to the glycosidyl bond. On the basis of modeling, the angular C5−H (antiGC) and C4−H (antiCG) strongly destabilize the *syn*-conformation and fix the heterocyclic rings in the *anti*-conformation. This makes antiGC unable to flip to a pseudo antiCG form (Figure 5b). The same argument applies to the selective binding of antiGC in an TFO to a G:C pair in a duplex. In addition, antiCG and antiGC cannot bind to A:T or T:A bases pairs because the donor/acceptor arrangement does not coincide with their Hoogsteen H-bonding arrangement.

The 2-aminoquinazoline ring system, designed to bind to A:T and T:A, has a pK_a of ~4.8,[9] which ensures that the ring N1-position will not be protonated at physiological pH. As discussed above for antiGC and antiCG, molecular modeling predicts that these quinazoline deoxynucleosides will adopt the *anti*-conformation around the C-glycosidyl bond. This makes the quinolin-4-yl and -5-yl substituted nucleosides in an oligomer different and unique in their presentation to the DNA major groove (Figure 5c).

Modeling Studies. The association of a strand of d(antiTA)$_4$ was modeled with a d(T)$_4$:d(A)$_4$ B-DNA duplex sequence. The antiTA oligomer was constructed from a B-DNA d(T)$_4$ oligomer with the thymine bases replaced with 2-aminoquinazolines without disturbing the structure of the deoxyribose backbone. Initially, the d(antiTA)$_4$ oligomer was manually docked with the T:A duplex so that the molecules were aligned with reasonable H-bond distances and angles. The structures were then minimized by treating the duplex and the antiTA oligomer as individual aggregates so their internal structures would not be perturbed by the force field. Hoogsteen H-bond distances and angles were gradually constrained down to 1.8−2.2 Å and 160−180°, respectively. This was accomplished by increasing the force constants associated with the different distance and angle constraints in a stepwise fashion. Orthogonal views of a final representative structure are shown in Figure 6. Importantly, the glycosidyl linkage between the antiTA base and the 2′-deoxyribose ring remains near center in the major groove at the different steps in the duplex.

Synthesis. The synthesis of the antiTA deoxyribose "nucleoside" shown in Figure 7 is based on a general method to stereospecifically prepare β-C-glycosides. The approach utilizes a protected ribofuranoid glycal[7] that is coupled with a halogenated heterocycle using a Pd-mediated Heck-type reaction. The method has been used to prepare a variety of C-glycosides in multigram amounts with yields in the range of 40−80%.[10,11] The conditions described to couple 2-amino-5-bromoquinazoline (**4**) with the furanoid glycal (Figure 7) reflect an effort to maximize yields by altering protecting group, base, solvent, and catalyst. The conversion of the quinazoline "deoxynucleoside" **7** into the protected phosphoramidite (**10**) followed standard procedures. Solid-phase synthesis was used to prepare the antiTA-modified oligomers OL-1, -2, and -5 (Table 1) and the coupling yields for the antiTA phosphoramidites was comparable to standard phosphoramidites (>99% based on trityl assay).

(9) Perrin, D. D. *Dissociation Constants of Organic Bases in Aqueous Solution*; Butterworth Press: London, 1965.

(10) Cheng, J. C.-Y.; Hacksell, U.; Davies, G. D., Jr. *J. Org. Chem.* **1985**, *50*, 2778−2780.

(11) (a) Davies, G. D., Jr. *J. Org. Chem.* **1992**, *57*, 4690−4696. (b) Farr, R. N.; Kwok, D.-I.; Davies, G. D., Jr. *J. Org. Chem.* **1992**, *57*, 2093-2100.

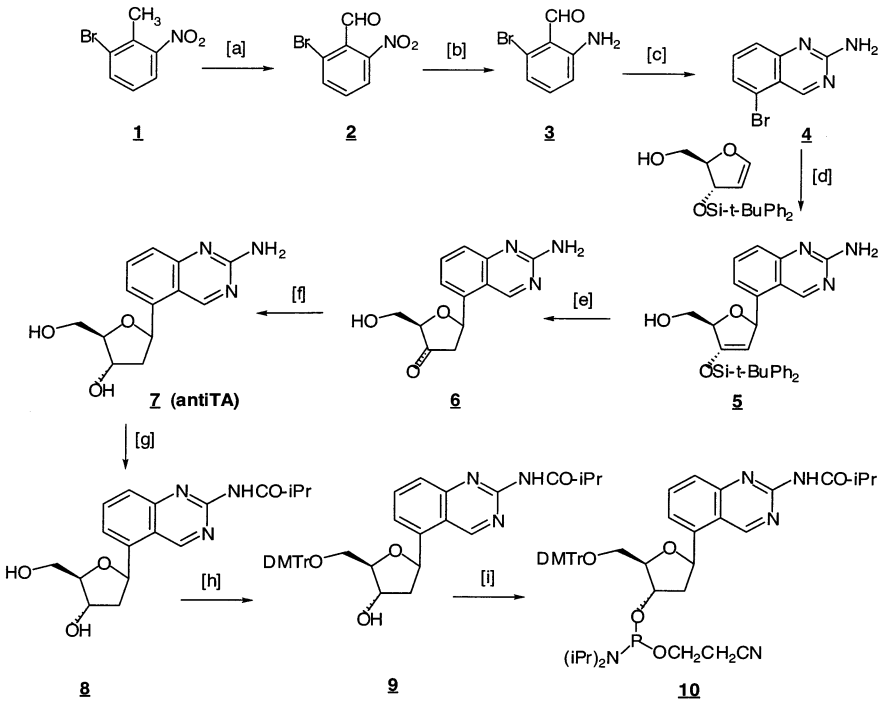

Figure 7. Synthesis of antiTA phosphoramidite (**10**): [a] (i) Br_2, *hν*, 145−150 °C; (ii) *N*,*N*-dimethyl-*p*-nitrosoaniline, EtOH, 0 °C; (iii) aqueous H_2SO_4, reflux; [b] Fe, aqueous HCl, reflux; [c] $NH_2C(=NH)NH_2$, 2-ethoxyethanol, 160−180 °C; [d] bis(dibenzylideneacetone)Pd(0), *tert*-Bu_3P/Et_3N, THF, reflux; [e] TBAF, 0 °C; [f] $NaHB(OAc)_3$, HOAc/MeCN, −23 °C; [g] $(i\text{-PrCO})_2O$, pyridine; [h] DMTrCl, pyridine, 0 °C; [i] 2-cyanoethyl *N*,*N*-diisopropylchlorophoramidite, *N*,*N*-diisopropylethylamine, CH_2Cl_2, 0 °C.

It was established that the 2-aminoquinazoline ring was stable to the coupling and deprotection conditions (data not shown). The oligomers were purified by reverse phase HPLC and their structures confirmed by MALDI-TOF MS.

Triplex Formation. An important factor in triplex stability is the stacking of the heterocyclic aromatic bases that is driven by hydrophobic effects.[12] In an effort to compare the stacking properties of antiTA to adenine, oligomers 5′-CGCGCG and 5′-N-CGCGCG (N = adenine or antiTA) were synthesized. The former is a perfect self-complementary duplex, while the later has a single 5′-adenine or -antiTA overhang. The T_M studies show an 8 °C increase in the T_M for the heptamer with antiTA or dA overhangs (T_M = 46 °C) relative to the hexamer (T_M = 38 °C), indicating that there is an equivalent stabilization due to stacking.[13]

To test the approach of building artificial bases with centralized glycosidic bonds to recognize Hoogsteen base pairing information, we constructed oligomers with antiTA that would form intramolecular triplexes. The formation of intramolecular triple-stranded structures is highly favored for entropic reasons[14] and allows studies with $d(T)_n$:$d(A)_n$ targets that form relatively unstable intermolecular triplexes.[15] In addition, the intramolecular approach provides a control over the orientation of the TFO sequence with respect to the duplex.

OL-1 and -2 (Table 1) provide a test of the stability of triplexes with antiTA bases and whether there is a preferred orientation as predicted from modeling (Figure 5a). Studies were performed with OL-3 and -4 in which a parallel third pyrimidine strand, as in OL-3, is required to form a stable pyridine-motif triplex. OL-5, which is the same as OL-1 except it contains a single T:A → A:T transversion in the duplex region, was synthesized to test the fidelity of duplex DNA recognition by the $(antiTA)_6$ sequence. OL-6 and -7 are hairpin duplexes with dangling 5′-C_5 stretches that cannot form triplexes.

The unfolding of duplex and/or triplex structures for OLs 1−7 was studied in 10 mM sodium phosphate buffer (pH 7.0) containing 50 or 200 mM NaCl by measuring the hyperchromicity at 260 and 350 nm as a function of temperature. Typically the extinction coefficient for the aromatic nucleobases increases as they unstack during the transition from duplex or triplex to random coils. The environment of adenine (λ_{max} 260 nm) and thymidine (λ_{max} 267 nm) can be monitored at 260 nm, but antiTA (λ_{max} 238 nm, ϵ = 21500) absorbs weakly at this wavelength (Figure 8). Fortunately antiTA has a unique absorption at 350 nm (ϵ = 2580) that is diagnostic of the environment of the quinazoline ring. The melting curves for the different oligomers in the presence of 50 or 200 mM NaCl were used to calculate the midpoint (T_M) for the transition of the triplex and/or duplex to random coil (Table 1). The curves for studies with 200 mM NaCl are shown in Figure 9.

As expected, OL-3, in which the purine strand of the duplex and the third $(T)_6$ strand are parallel, forms a stable triplex with a cooperative single transition (T_M, 22.7 °C) from triplex to random coil, and with approximately 23% hyperchromicity at 260 nm in 200 mM NaCl (Figure 9a). The T_M is 10 °C lower

(12) (a) Horne, D. A.; Dervan, P. B. *Nucl. Acids Res.* **1991**, *19*, 4963−4965. (b) Rougée, M.; Faucon, B.; Mergny, J. L.; Barcelo, F.; Giovannangéli, C.; Garestier, T.; Hélène, C. *Biochemistry* **1992**, *31*, 9269−9278. (c) Roberts, R. W.; Crothers, D. M. *Proc. Natl. Acad. Sci. U.S.A.* **1991**, *88*, 9397−9401.
(13) Kool, E. T,; Morales, J. C.; Guckian, K. M. *Angew. Chem., Int. Ed. Engl.* **2000**, *39*, 990−1009.
(14) (a) Plum, G. E.; Breslauer, K. J. *J. Mol. Biol.* **1995**, *248*, 679−695. (b) Rentzeperis, D.; Marky, L. A. *J. Am. Chem. Soc.* **1995**, *117*, 5423−5424. (c) Soto, A. M.; Loo, L.; Marky, L. A. *J. Am. Chem. Soc.* **2002**, *124*, 14355−14363.
(15) (a) Shea, R. G.; Ng, P.; Bischofberger, N. *Nucl. Acids Res.* **1990**, *18*, 4859−4866. (b) Pilch, D. S.; Levenson, C.; Shafer, R. H. *Proc. Natl. Acad. Sci. U.S.A.* **1990**, *87*, 942−946. (c) Kibler-Herzog, L.; Kell, B.; Zon, G.; Shinozuka, K.; Mizan, S.; Wilson, W. D. *Nucl. Acids Res.* **1990**, *18*, 3545−3555.

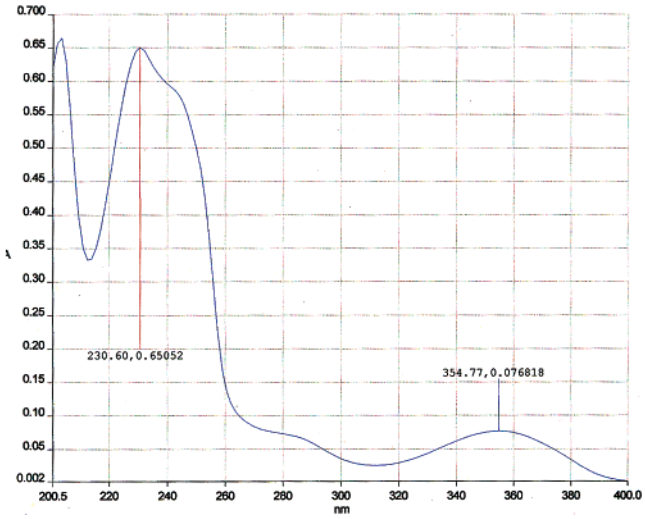

Figure 8. UV−vis spectrum of 70 μM antiTA (**7**) in 10 mM sodium phosphate buffer (pH 7.0).

in 50 mM NaCl (Table 1), but the hyperchromicity is unchanged. This T_M profile is the same as that previously reported.[14c] The appearance of transitions from triplex to duplex (T_M, 13.0 °C) and duplex to random coil (T_M, 59.4 °C) becomes evident (Figure 9b) upon addition of 1 equiv of netropsin, which binds in the minor groove and specifically stabilizes the duplex structure.[14,16] As expected, OL-4 shows no evidence for triplex formation upon the co-addition of netropsin because the T_6 sequence (either 5′ or 3′ of the A_6 stretch) and purine strand of the duplex are not parallel.[1a,17] At both low and high salt, the A_{260} melting curves of OL-6 and -7 are virtually identical to those of OL-4 in terms of T_M and hyperchromicity. Netropsin also increases the T_M values of OL-4, OL-6, and OL-7 because it binds in their A/T rich minor grooves. It should be noted that OL-3, which forms a triplex structure, OL-4, which does not, and OL-6, which cannot, have very similar T_M values (Table 1) and melting profiles (Figure 9a) in the absence of netropsin. However, due to the unstacking of the third strand from a triplex structure, the hyperchromicity is 21−23% for OL-3 versus 13−16% for OLs 4, 6, and 7 (Figure 9a).

Since the antiTA aminoquinazoline base has a weak absorption at 260 nm (Figure 8), it was anticipated that the unfolding of a triplex from OL-1 would result in a hyperchromicity only slightly larger than for OL-6, which cannot form a triplex. The hyperchromicity at 260 nm for OL-1 is 19%, which compares with 16% seen with OL-6. Significantly, at 350 nm only OL-1 shows a temperature-dependent hyperchromicity (10%) due to the unfolding of the $(antiTA)_6$ sequence from a triplex structure (Figure 9c). The co-addition of an equivalent of netropsin to the melt of OL-1 increases the T_M of the duplex region measured at 260 nm (Figure 9b). There is also some broadening of the melting curve at 350 nm (Figure 9d) that is indicative of a less cooperative triplex denaturation. Because of the less cooperative denaturation of the $(antiTA)_6$ tract, the accuracy of the T_M values is less precise. Despite this problem, the T_M values calculated for OL-1 at 260 and 350 nm are in general agreement and indicate an apparent concerted unfolding from triplex to random coil.

The antiTA strand in OL-2 does not have the required orientation relative to the duplex to form a triplex and has very different melting characteristics from OL-1. The hyperchro-

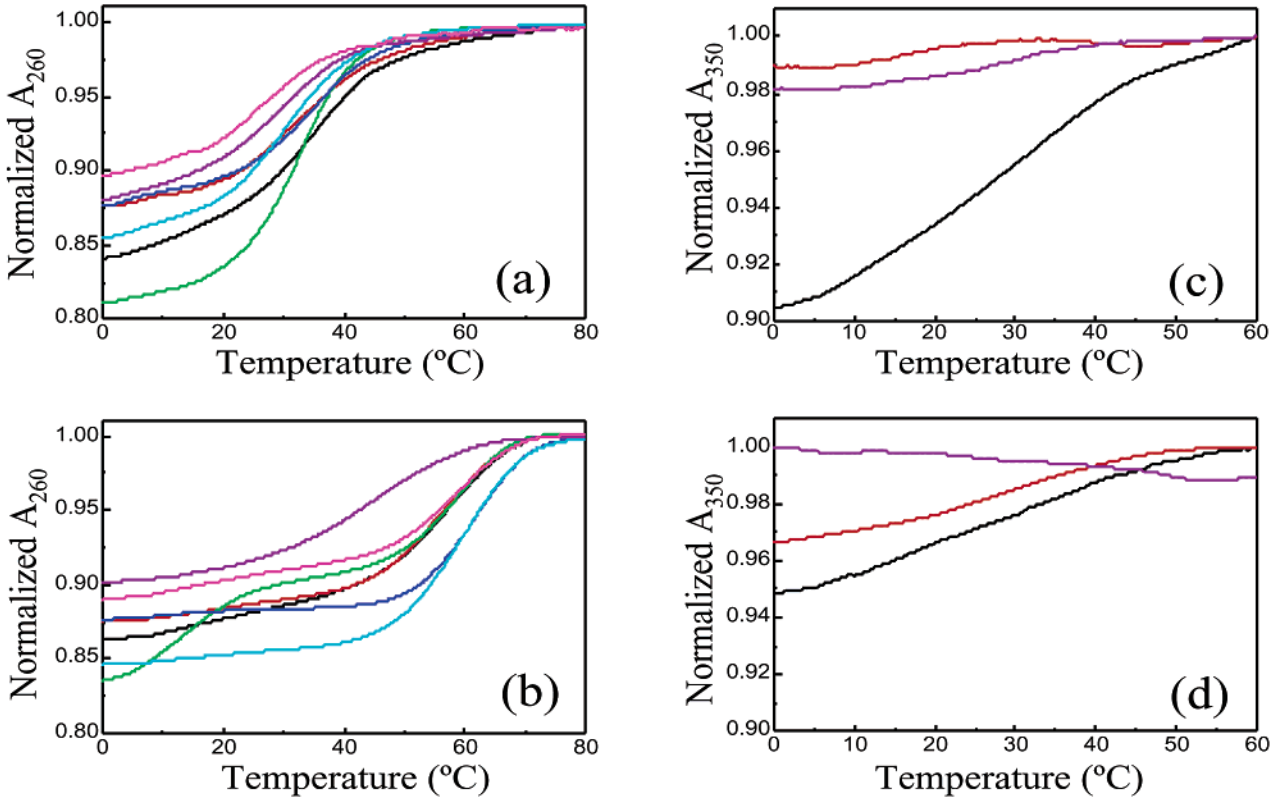

Figure 9. Thermal melting studies of OLs 1−7 (3−6 μM strand concentration) in 10 mM sodium phosphate buffer (pH 7.0) containing 200 mM NaCl: (a) 260 nm; (b) 260 nm with 1 equiv of netropsin; (c) 350 nm; (d) 350 nm with 1 equiv of netrospin (OL-1, black; OL-2, red; OL-3, green; OL-4, dark blue; OL-5, purple; OL-6, light blue; OL-7, magenta).

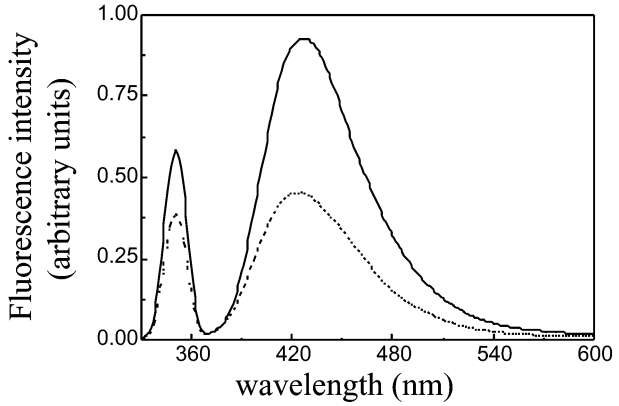

Figure 10. Fluorescence spectra of OL-1 (4 μM) in 10 mM sodium phosphate buffer (pH 7.0) containing 200 mM NaCl at 0 °C (solid line) and 70 °C (dashed line).

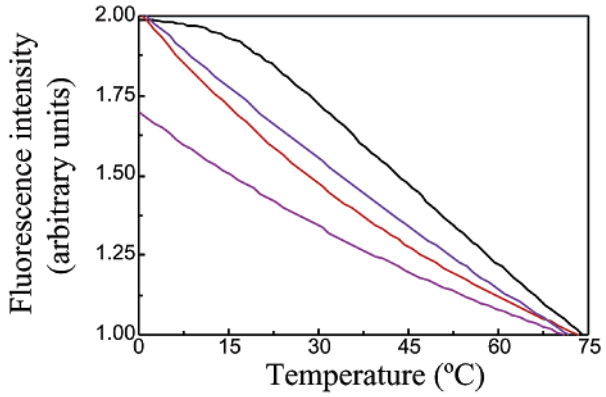

Figure 11. Effect of temperature on the fluorescence spectra of OLs 1, 2, and 5, and monomer **6** (3−5 μM strand concentration) in 10 mM sodium phosphate buffer (pH 7.0) containing 200 mM NaCl: OL-1, black; OL-2, red; OL-5, purple; monomer **6**, dark blue.

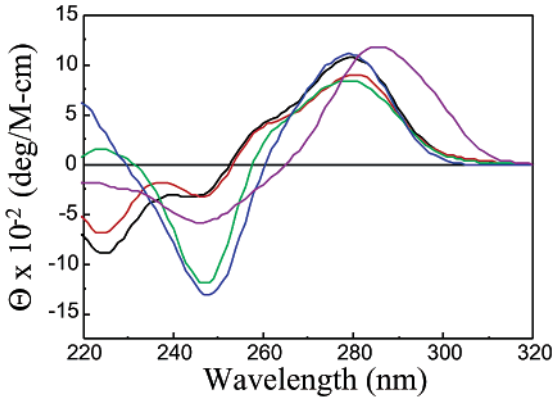

Figure 12. CD spectra of 6−8 μM strand concentration of OLs 1−5 in 10 mM sodium phosphate buffer (pH 7.0) containing 50 mM NaCl: OL-1 (black), OL-2 (red), OL-3 (green), OL-4 (dark blue), OL-5 (purple).

micity for OL-2 is similar to that of OL-1 at 260 nm (Figure 9a), but it shows no hyperchromicity at 350 nm (Figure 9c), indicating that it does not form a triplex. The orientational preference that allows OL-1, but not OL-2, to fold into a triple stranded structure is consistent with the design of the antiTA bases that permits discrimination between T:A and A:T base pairs in a duplex as defined in Figure 5a. Additional evidence that antiTA can discriminate between T:A and A:T base pair presentation is seen in the melting of OL-5, which is identical to OL-1 except it has a single T:A to A:T transversion in the duplex region. This sequence change decreases the hyperchromicity at 260 nm (Figure 9a) to that observed for duplex controls (OL-6 and -7). Moreover, at 350 nm no temperature-dependent hyperchromicity is observed for OL-5 (Figure 9c). Netropsin has no effect on the hyperchromicity of OL-2 or OL-5 (Figure 9d). Because OL-2 and OL-5 have the same 5′-(antiTA)$_6$ sequence as OL-1, the hyperchromicity seen in the melting of OL-1 cannot result from denaturation of some secondary structure adopted by the (antiTA)$_6$ sequence.

A prediction of the modeling of oligomers with antiTA substitutions is that the centralized backbone is incompatible with the backbone of natural bases and the formation of a mixed triplex TFO with natural and quinazoline bases is not possible. This was verified by incorporating a single antiTA residue in the fourth position from the 5′-terminus in the dT stretch in OL-3. This interruption by the antiTA blocked triplex formation as indicated by UV melting (data not shown).

The aminoquinazoline heterocycle shows a strong fluorescence emission spectrum at 425 nm when excited at 350 nm. The emission spectrum of OL-1 at 0 and 70 °C is shown in Figure 10, and while the emission maximum does not change, there is a decrease in the intensity of the emission at the higher temperature. The fluorescence emission intensity as a function of temperature was determined for OLs 1, 2 and 5, and for monomer **6** (Figure 7 for structure) and the results are shown in Figure 11. The curves for OL-2, OL-5, and **6** can be fitted to a first-exponential decay. In contrast, below 25 °C OL-1 has a very different sensitivity to increasing temperature. Above this temperature, the decrease in the 425 nm emission is similar to OL-2, OL-5, and monomer **6**. The transition temperature of approximately 25 °C is close to the T_M of 26.4 °C in 200 mM NaCl calculated from the UV−vis melting curve at 350 nm (Table 1). The biphasic temperature effect on fluorescence intensity seen with OL-1 is interpreted to reflect the melting of the anti(TA)$_6$ region out of a triplex and into a single-stranded form that can undergo rapid collisional quenching. Similar fluorescence changes have been observed in the melting of duplexes containing a modified fluorescent base.[18]

The CD spectra of OLs 1−7 were determined at 0 °C from 200 to 400 nm, although no bands were seen above 320 nm (Figure 12). The CD spectrum of OL-1 shows a positive band at 278 nm with a shoulder at 254 nm and negative bands at 248 and 223 nm. OL-2 has a CD spectrum very similar to that of OL-1, although the negative band at 223 nm is less intense. OL-3 and -4 show strong negative bands at 248 and 210 nm. OL-5, which has a mixed A/T Watson−Crick duplex sequence, also has a strong positive 278 nm band, but the negative band at 248 nm is much less pronounced. The CD spectra of OL-6 and -7 have positive bands at 274 nm and negative bands at 248 and 208 nm (data not shown). In general the CD spectra for the different sequences are not very diagnostic for structure.

(16) (a) Durand M. S.; Thuong, N. T.; Maurizot, J. C. *J. Biol. Chem.* **1992**, *267*, 24394−24399. (b) Park, Y. W.; Breslauer, K. J. *Proc. Natl. Acad. Sci. U.S.A.* **1992**, *89*, 6653−6657. (c) Wilson, W. D.; Tanious, F. A.; Mizan, S.; Yao, S.; Kiselyov, A. S.; Zon, G.; Strekowski, L. *Biochemistry* **1993**, *32*, 10614−10621.

(17) (a) Arnott, S.; Selsing, E. *J. Mol. Biol.* **1974**, *88*, 509−521. (b) Manzini, G.; Xodo, L. E.; Gasparotto, D.; Quadrifoglio, F.; van der Marel, G. A.; van Boom, J. H. *J. Mol. Biol.* **1990**, *213*, 833−843.

(18) (a) Lyckell, P.-O.; Gräslund, A.; Claesens, F.; McLaughlin, L. W.; Larsson, U.; Rigler, R. *Nucl. Acids Res.* **1987**, *15*, 9011−9025. (b)Wu, P.; Nordlund, T. M.; Gildea, B.; McLaughlin, L. W. *Biochemistry* **1990**, *29*, 6508−6514.

Conclusions

The UV−vis and fluorescence data indicate that antiTA can, as predicted, participate in the formation of a stable triplex that is sequence and orientation specific. Future studies incorporating the antiTA modification with antiAT, antiGC, and antiCG heterocyclic C-glycosides will be performed to determine if the centralization of the glycosidic bonds can provide a way to overcome the barrier for triplex formation in heteropurine/pyrimidine sequences.

Acknowledgment. This work was supported by NIH Grant RO1 CA29088, Nebraska Department of Health Grant 93-19, and Cancer Center Support Grant P30 CA36727 from the National Cancer Institute. We thank Greg Kubik of the Eppley Institute Molecular Biology Shared Resource for the synthesis of the oligomers and Ronald Shikiya for his technical help.

JA028033X